



Combined GPS/GLONASS global ionosphere mapping considering the GLONASS inter-frequency differential code bias

Qiang Zhang¹ · Jun Tao¹ · Xuanzuo Liu¹ · Zhigang Hu¹ · Qile Zhao^{1,2}

Received: 29 November 2022 / Accepted: 24 March 2023 / Published online: 10 April 2023
© The Author(s), under exclusive licence to Springer-Verlag GmbH Germany, part of Springer Nature 2023

Abstract

According to the frequency division multiple access (FDMA) technology of GLONASS, the receiver inter-frequency differential code bias (IFDCB) exists in the GLONASS dual-frequency geometry-free combination observable. This study specifically investigates the contribution of GLONASS data to global ionosphere mapping, especially considering the GLONASS receiver IFDCB. A “co-located GNSS stations” experiment shows that the GLONASS receiver IFDCB is distinguishable from the leveling error induced by the “carrier-to-code leveling” method, and the individual GLONASS receiver IFDCB for each satellite at one station should be considered. Based on this experiment, a modified ionospheric model for combined GPS and GLONASS global ionosphere mapping is proposed, in which the GLONASS satellite plus receiver DCB (SPRDCB) for each satellite-station link is directly estimated. The influence of the modified ionospheric model on the DCB estimation and the global ionospheric vertical total electron content (VTEC) map is comprehensively analyzed using data from the international GNSS service (IGS) network for day of year (DOY) 49–108, 2014. First, the modified ionospheric model can slightly improve the stability of the GPS satellite DCB. The GPS receiver DCB at most stations are higher than when only GPS data are used. Second, the neglect of the satellite-dependent part of the GLONASS receiver IFDCB may introduce an error of tens of TEC units (TECU) in the slant TEC (STEC) computation. Comparing to the conventional ionospheric model that ignores the GLONASS receiver IFDCB, the modified ionospheric model can significantly reduce the GLONASS residual errors. Third, the modified ionospheric model can improve the accuracy of the global ionosphere map (GIM) at most independent stations based on an external accuracy assessment test (or dSTEC test). We suggest considering the GLONASS receiver IFDCB in the combined GPS and GLONASS global ionosphere mapping, it will revise the inaccurate estimation induced by the conventional ionospheric model and result in reliable GIM and DCB products.

Keywords GPS · GLONASS · Global ionosphere mapping · Total electron content · Inter-frequency differential code bias

Introduction

Over the last two decades, the global navigation satellite system (GNSS) has become an advanced technique to monitor the Earth's ionosphere with its unprecedented high temporal and spatial sampling rate (Hernández-Pajares et al. 2011). Many efforts have been made to provide a high-precision and reliable global ionospheric map (GIM), since the

establishment of the ionospheric working group (IWG) of the international GNSS service (IGS) in 1998 (Feltens 2003; Hernández-Pajares et al. 2009). During the beginning phase, GIM vertical total electron content (VTEC) products were generated using dual-frequency GPS measurements (Juan et al. 1997; Mannucci et al. 1998; Schaer 1999). With the rapid development of GLONASS and multi-GNSS systems, GLONASS data, Galileo data and BeiDou navigation satellite system (BDS) data have also been incorporated into global ionospheric modeling (Ren et al. 2016; Yao et al. 2018; Hernández-Pajares et al. 2020; Brack et al. 2021).

In the extraction of ionospheric TEC from the raw dual-frequency measurements of GNSS data, the differential code bias (DCB) in satellite and receiver are the main systematic bias to be calibrated or estimated (Coco et al. 1991; Li et al. 2012). The code bias is assumed to be dependent on

✉ Zhigang Hu
zhigang.hu@whu.edu.cn

¹ GNSS Research Center, Wuhan University, No. 129 Luoyu Road, Wuhan 430079, China

² Collaborative Innovation Center of Earth and Space Science, Wuhan University, No. 129 Luoyu Road, Wuhan 430079, China

the signal frequency and on the signal modulation (Villiger et al. 2019). Because GPS, Galileo and BDS use the code division multiple access (CDMA) technology, the two frequencies for different satellites are the same, which means that only one DCB should be estimated in the receiver. In contrast to the CDMA-based systems, GLONASS uses frequency division multiple access (FDMA) technology to make the signals from individual satellites distinguishable (Wanninger 2012), which leads to different inter-frequency biases (IFBs) for both code and carrier phase observations. When we use dual-frequency GLONASS measurements to derive the ionospheric observables, there will exist the inter-frequency differential code bias (IFDCB) in the receiver. The receiver IFDCB is assumed to be frequency-dependent, in other words, the receiver IFDCBs for different GLONASS satellites with different frequencies are different. But in practice, the GLONASS receiver IFDCB is usually ignored for simplicity in multi-GNSS DCB determination (Wang et al. 2016; Liu et al. 2019) and the global ionospheric modeling (Li et al. 2015; Ren et al. 2016; Zhang and Zhao 2018).

In recent years, GLONASS IFBs in the code and carrier phase measurements have been investigated to improve positioning accuracy (Al-Shaery et al. 2013; Chen et al. 2017). The precise point positioning (PPP) accuracy was greatly improved during the convergence period when the GLONASS code IFBs were calibrated (Shi et al. 2013). Zhang et al. (2021) estimated the GLONASS code IFBs using ionospheric delay modeling and undifferenced uncombined PPP methods. However, this crucial issue concerning the GLONASS receiver IFDCB in global ionospheric modeling is rarely studied. Zhang et al. (2017a) proposed a two-step ionospheric modeling method with a priori IFDCB information to express the regional ionospheric VTEC distribution. In their method, a reference station with a good location and observation environment should be chosen, and a prior ionospheric product, such as a GIM product, should be introduced. Zhang et al. (2017b) investigated the influence of the GLONASS receiver IFDCB on DCB estimation and ionospheric modeling. In their global ionospheric modeling algorithm, the satellite and receiver DCB of GPS and GLONASS were corrected using predetermined DCB products, which were estimated using an existing GIM product. In addition, their GLONASS receiver IFDCB was set per frequency channel, and station-dependent frequency channel constraints should be introduced. As mentioned above, both proposed methods require an existing GIM product, and their results might be affected by the prior ionospheric information or the station-dependent frequency channel constraints.

In the context of the IGS IWG, there are seven Ionosphere Associate Analysis Centers (IAACs) providing GIM products with different techniques (Roma-Dollase et al. 2018). The seven IAACs include the Jet Propulsion

Laboratory (JPL), Center for Orbit Determination in Europe (CODE), European Space Agency/European Space Operations Center (ESA/ESOC), Universitat Politècnica de Catalunya (UPC), Natural Resources Canada (NRCan), Chinese Academy of Sciences (CAS) and Wuhan University (WHU). JPL introduced the GLONASS observables to produce the global VTEC maps in early 2015 and estimated a separate bias for each GLONASS receiver-to-satellite pair (Vergados et al. 2016). CODE has added GLONASS data to its GIM product since 2003 (IGSMail 4371, 2003), but the GLONASS receiver IFDCB was ignored at that time. From June 2016, instrumental biases with respect to each involved GNSS code observable were modeled with one set of bias parameters for each satellite-station link in the case of GLONASS (Villiger et al. 2019). ESA/ESOC, NRCan, CAS and WHU have also included the GLONASS data in their GIM generation, but the GLONASS data were processed similarly to the GPS data (Feltens 2007; Ghoddousi-Fard 2014; Li et al. 2015; Zhang and Zhao 2018). UPC used only dual-frequency carrier phase GPS data to map the global ionosphere with the TOMION dual-layer voxel model (Hernández-Pajares et al. 1999). Although most IAACs have added GLONASS data, only JPL and CODE have considered the GLONASS receiver IFDCB in recent years. To our knowledge, very few public investigations have specifically been performed on the influence of GLONASS data on global ionospheric modeling. Therefore, it is necessary to investigate the contribution of GLONASS data to global ionospheric modeling, especially considering the GLONASS receiver IFDCB characteristics.

This study complements the efforts of previous research by analyzing the contribution of GLONASS data to DCB estimation and global ionospheric modeling. We propose a modified method for combined GPS and GLONASS global ionosphere mapping considering the GLONASS receiver IFDCB. Following this introduction, the characteristics of the GLONASS receiver IFDCB are analyzed first. Then, global ionosphere mapping with and without GLONASS receiver IFDCB consideration is presented. The influence of the GLONASS data on the GPS satellite and receiver DCB estimation, the GLONASS residuals, and the global ionospheric VTEC map are provided. Finally, a summary and conclusions are given.

Characteristics of the GLONASS receiver IFDCB

The basic observations of the GNSS pseudorange and carrier phase are described as follows (Zhang and Zhao 2018):

$$\begin{cases} P_{f,i}^k = \rho_i^k + c\delta_i - c\delta^k + I_{f,i}^k + T_i^k + cb_{f,P,i} + cb_{f,P}^k + m_{f,P,i}^k + \epsilon_P \\ L_{f,i}^k = \rho_i^k + c\delta_i - c\delta^k - I_{f,i}^k + T_i^k + \lambda_f N_{f,i}^k + m_{f,L,i}^k + \epsilon_L \end{cases} \quad (1)$$

where $P_{f,i}^k$ and $L_{f,i}^k$ are the pseudorange and carrier phase measurements from receiver i to satellite k at frequency f with wavelength λ_f ; ρ_i^k is the geometric distance; c is the speed of light in a vacuum; δ_i and δ^k are the receiver and satellite clock biases, respectively; $I_{f,i}^k$ is the dispersive ionospheric delay in both the pseudorange (the delay) and the carrier phase (the advance); T_i^k is the nondispersive tropospheric delay; $b_{f,P,i}$ and $b_{f,P}^k$ are the code biases in the receiver and satellite, respectively; $N_{f,i}^k$ is the float carrier phase ambiguity in cycles (including integer ambiguity and uncalibrated phase delays in the receiver and satellite); $m_{f,P,i}^k$ and $m_{f,L,i}^k$ are multipath errors in code and phase, respectively; and ϵ_P and ϵ_L are the observational noises.

From dual-frequency GNSS observation equations, geometry-free measurements can be obtained by taking the difference between two given frequencies, as follows:

$$\begin{cases} P_{4,i}^k = P_{1,i}^k - P_{2,i}^k = I_{4,i}^k + cDCB_i + cDCB^k \\ L_{4,i}^k = L_{1,i}^k - L_{2,i}^k = -I_{4,i}^k + \lambda_1 N_{1,i}^k - \lambda_2 N_{2,i}^k \end{cases} \quad (2)$$

where $I_{4,i}^k = I_{1,i}^k - I_{2,i}^k$ is the combined ionospheric delay and $DCB_i = b_{1,P,i} - b_{2,P,i}$ and $DCB^k = b_{1,P}^k - b_{2,P}^k$ are the differential code biases in the receiver and satellite, respectively. The multipath effect and noise are not included in (2) for clarity.

Both the pseudorange and carrier phase measurements are used to extract the ionospheric observables. The precision of the carrier phase is approximately two orders of magnitude higher than that of the pseudorange, but it is affected by the unknown ambiguities. To acquire high-precision ionospheric information, a technical method called carrier-to-code leveling (CCL) is usually applied (Zhang et al. 2018). The leveled carrier phase measurement can be expressed as follows (Ciraolo et al. 2007):

$$\tilde{L}_{4,i}^k = -L_{4,i}^k + \left\langle L_{4,i}^k + P_{4,i}^k \right\rangle_{arc} = I_{4,i}^k + cDCB_i + cDCB^k \quad (3)$$

where $\left\langle L_{4,i}^k + P_{4,i}^k \right\rangle_{arc}$ is the average in a continuous arc.

The CCL method is widely used in global ionosphere mapping, but the leveled carrier phase ionospheric observables may be affected by the noise and multipath errors present in the code observations. We used “co-located GNSS stations” to assess the effects of systematic errors on the leveled carrier phase ionospheric observables. The co-located GNSS stations in this context indicate that two receivers are connected to the same antenna through an antenna splitter. The slant TEC (STEC) can be considered equal between the two stations. The systematic errors are

arc-dependent errors, also called “leveling error” (Ciraolo et al. 2007). With this experiment, the leveling error of the GLONASS data is compared to that of the GPS data, and the characteristics of the GLONASS receiver IFDCB can be found.

The leveled carrier phase measurement in (3) is extended to include both GPS and GLONASS data:

$$\begin{cases} \tilde{L}_{4,i}^{G,k} = I_{4,i}^{G,k} + c(DCB_{G,i} + DCB^{G,k}) \\ \tilde{L}_{4,i}^{R,l} = I_{4,i}^{R,l} + c(DCB_{R,i}^l + DCB^{R,l}) \end{cases} \quad (4)$$

where G stands for GPS, R stands for GLONASS, i denotes receiver, k and l denotes satellites; $DCB_{G,i}$ and $DCB^{G,k}$ are the GPS receiver DCB and satellite DCB, respectively; $DCB_{R,i}^l$ and $DCB^{R,l}$ are the GLONASS receiver DCB and satellite DCB, respectively. Comparing with the GPS receiver DCB, the GLONASS receiver DCB are dependent on satellite or frequency. Therefore, the GLONASS receiver DCB is called GLONASS receiver IFDCB hereafter.

If we make a single difference in the measurements from the same satellite between the two stations, the ionospheric delay and the satellite DCB can be canceled. The single-differenced (SD) measurements from stations i and j are described as follows:

$$\begin{cases} \tilde{L}_{4,ij}^{G,k} = cDCB_{G,i} - cDCB_{G,j} = cDCB_{G,ij} \\ \tilde{L}_{4,ij}^{R,l} = cDCB_{R,i}^l - cDCB_{R,j}^l = cDCB_{R,ij}^l \end{cases} \quad (5)$$

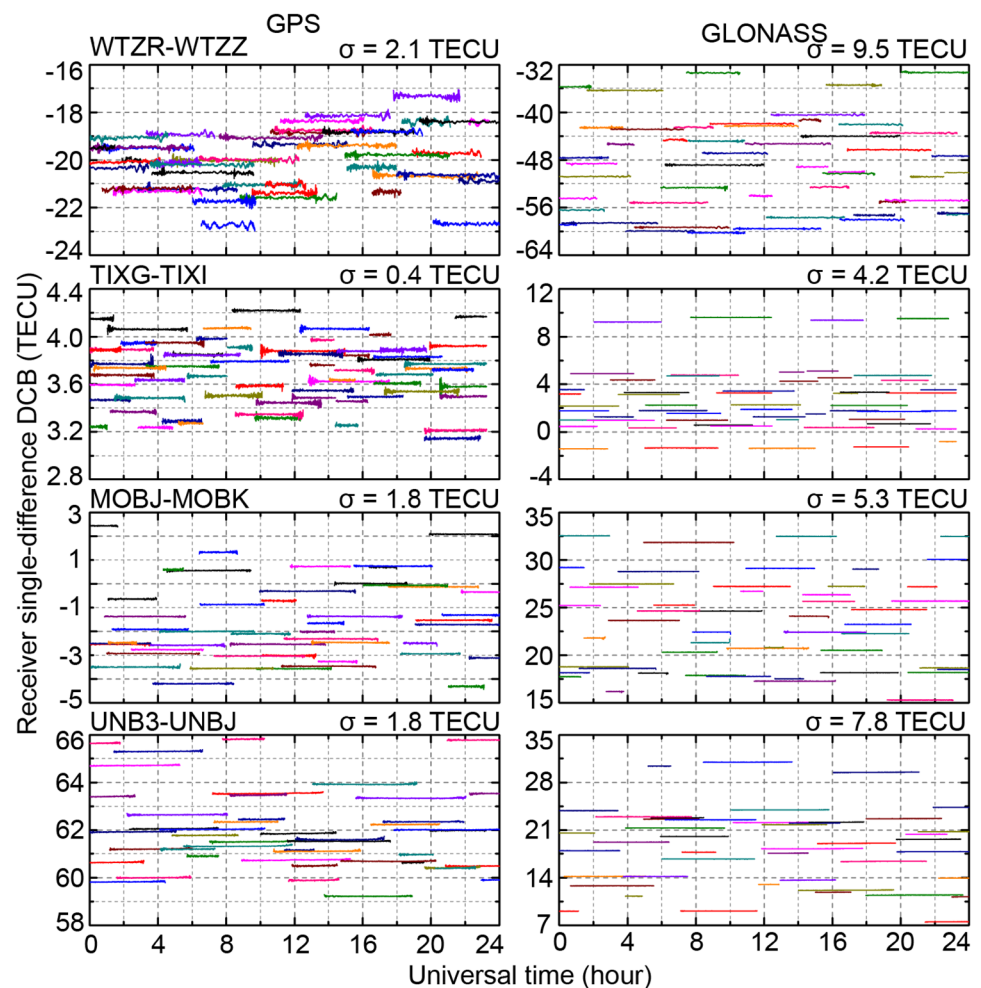
where $DCB_{G,ij}$ stands for the single-differenced GPS receiver DCB and $DCB_{R,ij}^l$ stands for the single-differenced GLONASS receiver IFDCB from satellite l .

It is clear that the GLONASS receiver SD-IFDCBs are dependent on different satellites, while the GPS receiver SD-DCBs for all satellites are theoretically the same. In fact, due to the leveling error, it is not clear whether we can distinguish the GLONASS receiver IFDCB from the leveling error.

We selected four co-located GNSS stations from the IGS network. Each set of collocated stations had different receivers but the same type of antenna: WTZR and WTZZ (LEICA GR25 and JAVAD TRE_G3TH DELTA, LEIAR25.R3), TIXG and TIXI (TPS ODYSSEY_E and JPS EGGDT, TPSCR3_GGD), MOBJ and MOBK (JPS LEGACY and JPS EGGDT, JPSREGANT_SD_E1), UNB3 and UNBJ (TRIMBLE NETR9 and TPS LEGACY, TRM57971.00).

The GPS and GLONASS data from day of year (DOY) 49 to 79, 2014, were collected and analyzed. Figure 1 shows the receiver SD-DCBs from different satellites for GPS and GLONASS on DOY 64, 2014. For the GPS receiver SD-DCBs, the arc-to-arc spread reaches peak-to-peak values of approximately 6, 1, 5 and 5 TEC

Fig. 1 Receiver single-difference DCBs during one day for GPS (left) and GLONASS (right) on DOY 64, 2014. The different colors represent different satellites and σ is the leveling error



units (TECU) for WTZR-WTZZ, TIXG-TIXI, MOBJ-MOBK and UNB3-UNBJ, respectively. The corresponding leveling errors are approximately $(6/\sqrt{2})/2 \approx 2.1$, $(1/\sqrt{2})/2 \approx 0.4$, $(5/\sqrt{2})/2 \approx 1.8$ and $(5/\sqrt{2})/2 \approx 1.8$ TECU, respectively, which are similar to previous studies (Nie et al. 2018). For the GLONASS receiver SD-DCBs, the peak-to-peak values are approximately 27, 12, 15 and 22 TECU, which lead to leveling errors of 9.5, 4.2, 5.3 and 7.8 TECU, respectively. In these cases, the GLONASS leveling errors are at least three times larger than the GPS leveling errors. If we assume the magnitude of the GPS leveling error as the error introduced by the CCL method, the very large GLONASS leveling error is actually induced by the different GLONASS receiver IFDCBs.

The daily values of the WTZR-WTZZ receiver SD-DCBs over one month are shown in Fig. 2. We arbitrarily selected three satellites for each system, such as G02, G16 and G21 for GPS and R02, R16 and R21 for GLONASS. The SD-DCBs for the three GPS satellites are nearly the same and consistent with the expected theoretical results. While the SD-DCBs for the three GLONASS satellites are obviously different, they are -41.5 , -46.1 and -58.9 TECU for R02,

R16 and R21, respectively. Both the GPS SD-DCBs and the GLONASS SD-DCBs show good stability over one month. Comparing the GLONASS SD-DCBs with the GPS SD-DCBs, we can confirm that the GLONASS receiver IFDCB is distinguishable from leveling error and cannot be ignored in the data processing.

A previous study reported that the GLONASS code IFBs have correlations with the receiver type, the antenna type and the frequency (Shi et al. 2013). The four co-located stations are equipped with different receiver types and the same antennas in this experiment. It is important to investigate the correlation between the GLONASS receiver IFDCB and the frequencies. Figure 3 shows the mean value and standard deviation (STD) of the GLONASS receiver SD-DCBs at the four co-located stations. The SD-DCBs at WTZR-WTZZ and UNB3-UNBJ are frequency-dependent, while those at MOBJ-MOBK have no correlation with the frequency channel. In general, the SD-DCBs are nearly the same on the same frequency channel, and a previous study was performed on this basis (Zhang et al. 2017b). However, it is also observed that even with a same frequency channel, the difference in the SD-DCBs between

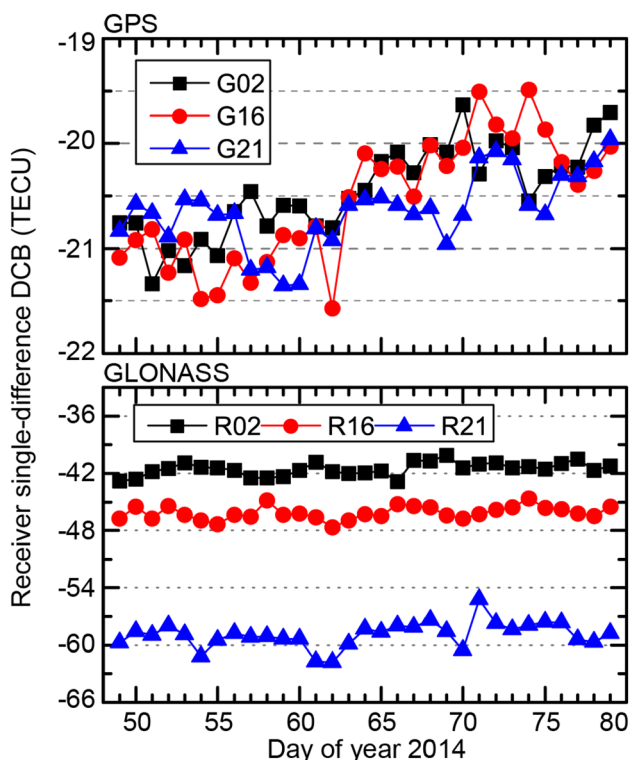


Fig. 2 Daily WTZR-WTZZ receiver single-difference DCBs for GPS satellites (G02, G16, G21) and GLONASS satellites (R02, R16, R21) from DOY 49 to 79, 2014

two different satellites can reach up to 5 TECU. To describe the GLONASS receiver IFDCB precisely, we suggest estimating individual receiver IFDCB for each GLONASS satellite at one station. In other words, the GLONASS receiver IFDCB is considered satellite-dependent in contrast to the previous frequency-dependent (Zhang et al. 2017b).

Global ionosphere mapping with and without GLONASS IFDCB consideration

The geometry-free ionospheric delay in (3) can be expressed using Taylor approximation, and the first-order term (with a dependence on f^{-2}) accounts for more than 99.9% of the total ionospheric delay (Hernández-Pajares et al. 2011). The geometry-free ionospheric delay can be expressed without the higher-order ionospheric delay as the following good approximation:

$$I_{4,i}^k = 40.28 \cdot \left(\frac{1}{f_1^2} - \frac{1}{f_2^2} \right) \cdot STEC_i^k \tag{6}$$

where $STEC_i^k$ is the slant total electron content from receiver i to satellite k .

An infinitely thin shell at an altitude of 450 km above Earth is assumed where the free electrons are concentrated for simplicity. The signal path and the thin shell intersect at a point that is called the ionosphere pierce point (IPP). The STEC along the signal path should be converted to VTEC through a modified single-layer model mapping function. Then, the global VTEC in the spatial and temporal domains can be represented using the well-known spherical harmonic (SH) expansion model (Schaer 1999). The spherical harmonic expansion model and mapping function are expressed as follows:

$$\begin{cases} VTEC(\beta, s) = \sum_{n=0}^{n_{max}} \sum_{m=0}^n \tilde{P}_{nm}(\sin \beta)(C_{nm} \cos(ms) + S_{nm} \sin(ms)) \\ STEC = M(z) \cdot VTEC \\ M(z) = 1 / \cos(\arcsin(R \sin(\alpha z) / (R + H))) \end{cases} \tag{7}$$

where $VTEC(\beta, s)$ is the vertical TEC; β and s are the latitude and longitude of the IPPs in the solar-geomagnetic reference frame, respectively; \tilde{P}_{nm} is the normalized associated Legendre function with degree n and order m , n_{max} is set as 15 in this study; C_{nm} and S_{nm} are the SH coefficients to be estimated; z is the satellite zenith at the station; R (~ 6371 km) is the radius of the Earth; H (~ 506.7 km) is the altitude of the ionosphere thin shell for the mapping function; and α is a correction factor that is set to 0.9782.

If we do not consider the GLONASS receiver IFDCB, we estimate only one GLONASS receiver DCB for one station. The term $DCB_{R,i}^l$ in (4) is replaced with the term $DCB_{R,i}$. To separate the receiver DCB from the satellite DCB, a zero-mean constraint on the satellite DCB for each system is introduced (Montenbruck et al. 2014). The global ionosphere mapping using combined GPS and GLONASS data without considering the GLONASS receiver IFDCB (conventional model) can be expressed as follows:

$$\begin{cases} \tilde{I}_{4,i}^{G,k} = F(X_{SH}) + c(DCB_{G,i} + DCB^{G,k}) \\ \tilde{I}_{4,i}^{R,l} = F(X_{SH}) + c(DCB_{R,i} + DCB^{R,l}) \\ \sum_{k=1}^{n_{sat}} DCB^{G,k} = 0 \\ \sum_{l=1}^{m_{sat}} DCB^{R,l} = 0 \end{cases} \tag{8}$$

where $F(X_{SH})$ stands for the SH expansion model and X_{SH} stands for the SH coefficients.

According to (8), the estimated parameters include the spherical harmonic coefficients, the DCBs for the GPS satellite and receiver and the DCBs for the GLONASS satellite and receiver. Usually, we divide one day into several

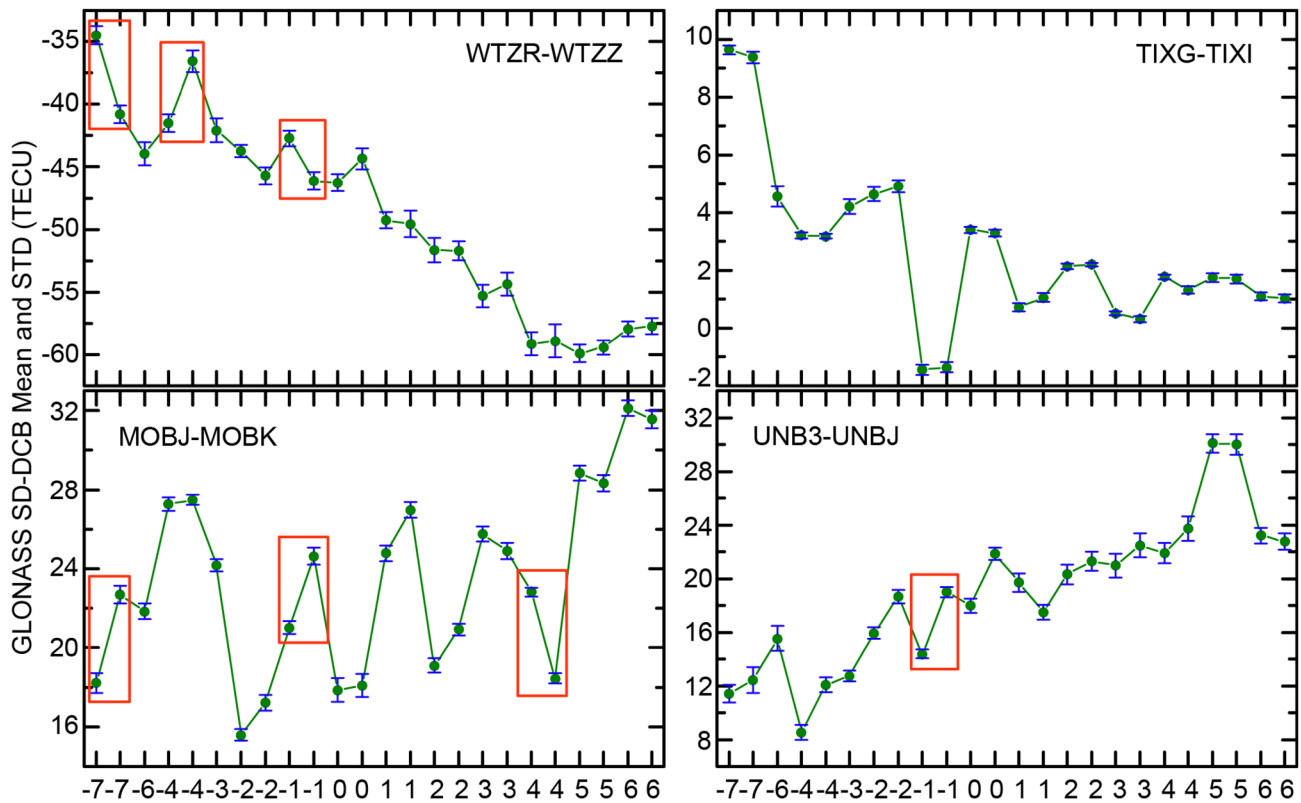


Fig. 3 Mean value and standard deviation of the GLONASS receiver SD-DCBs at the four co-located stations. The large differences between two satellites with a same frequency channel are labeled

with red rectangle in WTZR-WTZZ, MOBJ-MOBK and UNB3-UNBJ stations. The GLONASS satellites are listed in order of the frequency channel

sessions, and one pair of spherical harmonic coefficients is estimated for one session (Zhang and Zhao 2019). The session length is set to 2 h, and 13 pairs of spherical harmonic coefficients are estimated. If we assume that the numbers of GPS stations, GPS satellites, GLONASS stations and GLONASS satellites are 280, 32, 190 and 24, respectively, the total number of estimated parameters is 3854.

When we consider the GLONASS receiver IFDCB, the individual GLONASS receiver IFDCB for each satellite should be estimated at one station. The zero-mean constraint on the satellite DCB for the GPS still works, but it does not work for the GLONASS. A previous study (Zhang et al. 2017b) proposed additional frequency channel constraints to separate the GLONASS satellite DCB and the GLONASS receiver IFDCB. This method depends on the stations selected, i.e., when the stations change, the estimated values belong to different datums. Considering the global ionosphere modeling using a datum-consistent method, we propose estimating the sum of the GLONASS satellite DCB and the GLONASS receiver IFDCB directly, i.e., the GLONASS satellite plus receiver DCB (SPRDCB) for each satellite-station link. The global ionosphere mapping using combined GPS and GLONASS data with

consideration of the GLONASS receiver IFDCB (modified model) can be expressed as follows:

$$\begin{cases} \tilde{L}_{4,i}^{G,k} = F(X_{SH}) + c(\text{DCB}_{G,i} + \text{DCB}^{G,k}) \\ \tilde{L}_{4,i}^{R,l} = F(X_{SH}) + c\text{SPRDCB}_{R,i}^l \\ \sum_{k=1}^{n_{\text{sat}}} \text{DCB}^{G,k} = 0 \end{cases} \quad (9)$$

where $\text{SPRDCB}_{R,i}^l$ stands for the GLONASS satellite-station link SPRDCB. Our method does not separate the GLONASS satellite DCB and the GLONASS receiver IFDCB. It should be mentioned that when we speak of the consideration of the GLONASS receiver IFDCB, it means that we estimate the GLONASS satellite-station link SPRDCB hereafter.

For each GLONASS station, we should estimate every satellite-station link SPRDCB, and the number of estimated parameters increases rapidly. Compared with the conventional model in (8), the total number of estimated parameters of the modified model is 8200, which is approximately twice as large. The computation efficiency of the global ionosphere mapping is strongly related to the number of estimated parameters. Thanks to the application of parallel

computing techniques (Zhang and Zhao 2018) in global ionosphere modeling, this shortcoming of the modified model can be overcome.

Data processing

We selected GNSS observations from DOY 49 to 108, 2014, in our experiment. This period was during solar cycle 24 and was under strong solar activity conditions. The observations were collected from approximately 280 globally distributed IGS stations. The distribution of the GPS and GLONASS stations and the IPPs for both systems on DOY 75, 2014, are shown in Fig. 4.

Generally, most of the stations are distributed on land, especially on the European continent. Only a few stations are located on oceans. All stations can collect GPS data, but only 66% can track GLONASS satellites. The IPPs derived from both the GPS and the GLONASS from 00:00 to 04:00 universal time coordinated (UTC) are shown in the bottom plot. In the geographic-fixed coordinate system, the IPPs are distributed around the stations, and many data gaps can be observed over the oceans. The coordinate system is usually transformed from the earth-fixed to the solar-fixed to utilize the high correlation of the ionospheric activity with the position of the sun. Due to the rotation of the Earth, the ground-based GNSS stations resemble scanners to observe the ionosphere. As a consequence, the IPPs in the solar-fixed system are distributed more evenly (Zhang and Zhao 2023). Apparently, adding the GLONASS data helps increase the

number of IPPs at most stations. According to the statistics, the number of IPPs increases by approximately 50% when 9 GPS satellites and 6 GLONASS satellites are observed simultaneously. The GPS satellite inclination is 55° , while the GLONASS satellites have a higher inclination (64.8°) (Afraimovich and Yasukevich 2008). At high latitudes, GLONASS satellites are observed at higher elevations, decreasing the influence of horizontal ionospheric gradients and, consequently, enabling more accurate TEC representations over individual high-latitude stations.

Results and analysis

We analyzed the contribution of the GLONASS data to DCB estimation and global ionospheric modeling. The global ionosphere mapping using only GPS data is labeled GPS. The global ionosphere mapping using GPS and GLONASS data with and without the GLONASS receiver IFDCB consideration are labeled GRW and GRN, respectively. In the GPS solution, the SH coefficients with the GPS satellite DCB and GPS receiver DCB are estimated. In the GRN solution, the SH coefficients with the GPS satellite DCB, the GPS receiver DCB, the GLONASS satellite DCB and the GLONASS receiver DCB are estimated using (8). In the GRW solution, the SH coefficients with the GPS satellite DCB, the GPS receiver DCB and the GLONASS satellite-station link SPRDCB are estimated using (9). This section presents the influence of GLONASS data and receiver IFDCB consideration on the GPS satellite and receiver DCB estimation, the GLONASS satellite-station link SPRDCB and the global ionospheric VTEC map, respectively.

Influence on the GPS satellite and receiver DCB estimation

The GPS satellite and receiver DCBs are estimated simultaneously with the global ionospheric model parameters. The introduction of GLONASS data influences the ionospheric model and indirectly affects the GPS satellite and receiver DCBs. Figure 5 shows the averaged GPS satellite DCB differences between the three solutions, i.e., GPS, GRN, and GRW, from DOY 49 to 108, 2014. When the GLONASS data are added, the GPS satellite DCB differences between the GRN and GPS range from -0.03 to 0.02 ns. When the GLONASS receiver IFDCB is considered, the GPS satellite DCB differences between the GRW and GPS decrease slightly. The GPS satellite DCB differences between the GRW and GRN are also within 0.03 ns, and the maximum value is 0.025 ns. Compared with the magnitude of the GPS satellite DCB values (from -10.74 to 8.61 ns), the magnitude of the DCB differences is very small. The ratios between the DCB differences and the absolute DCB values

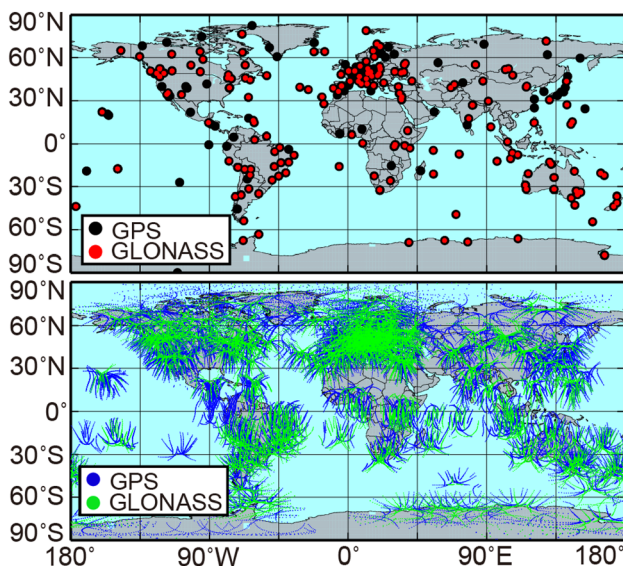


Fig. 4 Distribution of the selected IGS stations on DOY 75, 2014, and the IPP distribution from 00:00 to 04:00 UTC. The black (blue) and red (green) dots represent the GPS and GLONASS, respectively, in the top (bottom) plot

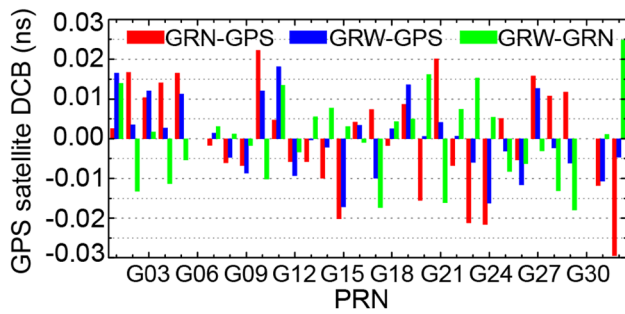


Fig. 5 Averaged GPS satellite DCB differences between the three solutions from DOY 49 to 108, 2014. The red, blue and green represent the differences between the GRN and GPS, between the GRW and GPS, and between the GRW and GRN, respectively

are less than 2%. The result indicates that the inclusion of the GLONASS data has little influence on the GPS satellite DCB values.

The DCB monthly stability (Wang et al. 2016) is usually used to describe the precision of DCB estimations. Figure 6 shows the GPS satellite DCB monthly stability. In general, the GPS satellite DCB stabilities are better than 0.16 ns, and they are less than 0.08 ns for most satellites. When the GLONASS data are added, the stabilities are improved by 3.47% and 3.79% on average for the GRN solution and the GRW solution, respectively. The maximum improvement is approximately 17% for G29 with the GRW solution. It is also observed that the stabilities for G02 and G28 become worse when the GLONASS data are added, but this deterioration is reduced with the GRW solution compared to the GRN solution. It is confirmed that the GLONASS data help to improve the stability of the GPS satellite DCB, especially when considering the GLONASS receiver IFDCB.

Figure 7 shows the averaged GPS receiver DCB differences between the GPS solution, the GRN solution and the GRW solution from DOY 49 to 108, 2014. The receivers are listed in order of station latitude. For most stations, the

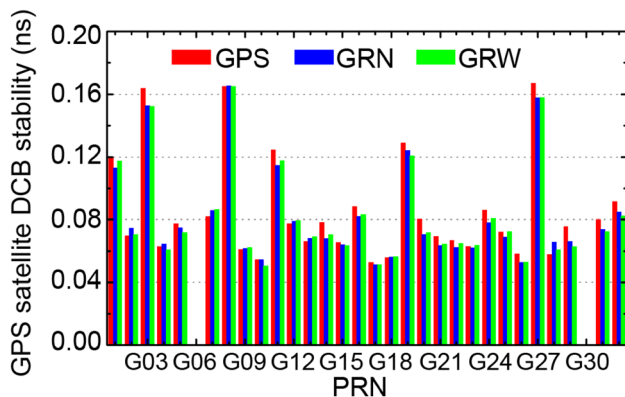


Fig. 6 GPS satellite DCB monthly stability. Red, blue and green represent the GPS, GRN and GRW, respectively

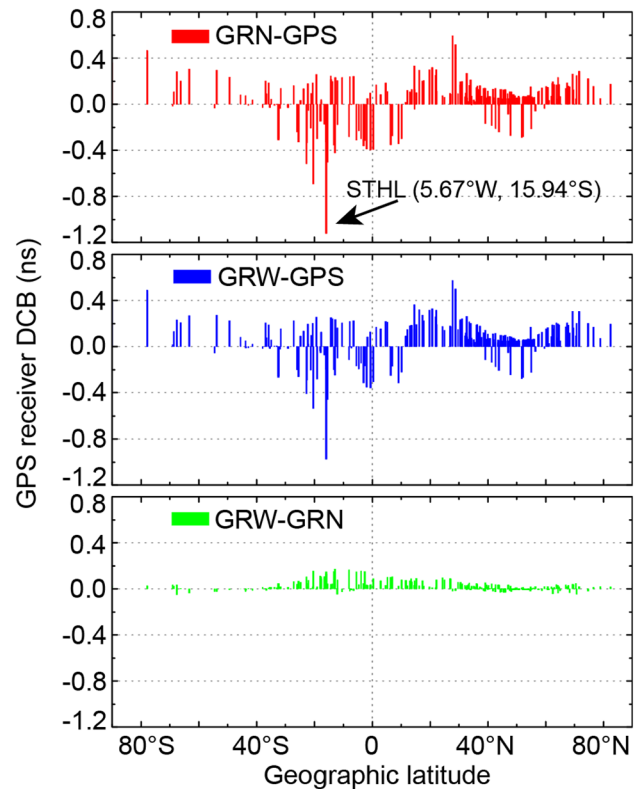
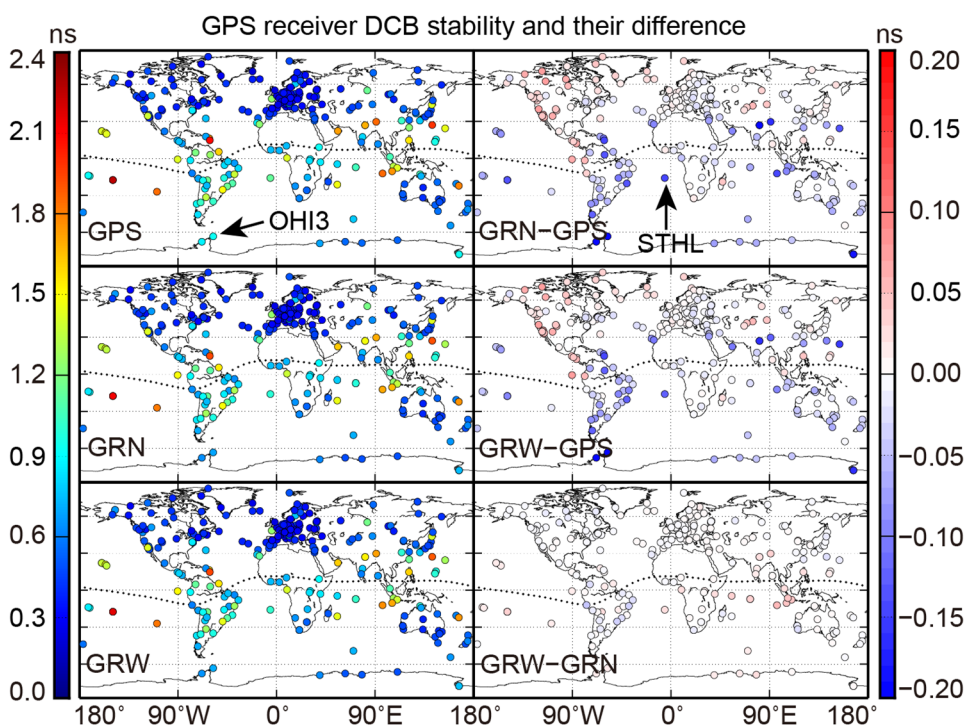


Fig. 7 Averaged GPS receiver DCB differences between the three solutions from DOY 49 to 108, 2014. Red, blue and green represent the differences between the GRN and GPS, between the GRW and GPS, and between the GRW and GRN, respectively. The stations are listed in order of latitude from the southern hemisphere to the northern hemisphere

DCB differences between the GRN (or GRW) and GPS range from -0.4 to 0.4 ns. The inclusion of the GLONASS data increases the GPS receiver DCBs at 77% of the stations compared to when only GPS data are used. In the northern hemisphere, most GPS receiver DCBs increase. The reduced receiver DCBs are generally located at low latitudes in the southern hemisphere. A remarkable minimum value of -1.12 ns is observed at station STHL (5.67° W, 15.94° S). This station is located on Saint Helena in the Southern Atlantic Ocean, where very few stations are distributed. It is believed that the inclusion of the GLONASS data has a large influence in regions where GPS data are sparsely distributed. The GPS receiver DCB values with the GRW solution are larger than those with the GRN solution, but the differences are generally less than 0.2 ns. Compared with the influence of the GLONASS data on the estimation of the GPS receiver DCB, the influence of the GLONASS receiver IFDCB is much smaller.

The GPS receiver DCB monthly stability at each station of the three solutions and their difference are shown in Fig. 8. In the left panel, the blue indicates small value and

Fig. 8 GPS receiver DCB monthly stability and the difference between the GPS, GRN and GRW solutions



the red indicates large value. While in the right panel, the blue indicates stability improvement, and the red indicates deterioration. The GPS receiver DCB stability over time is latitudinally dependent and ranges from 0.21 to 2.26 ns. The receiver DCB stabilities at low latitudes are significantly larger than that at middle and high latitudes. According to the statistics, the GPS receiver DCB stabilities at 60% of the stations are improved when the GLONASS data are added. Most stations in the southern hemisphere show stability improvement, and the maximum value of 0.24 ns (approximately 26%) is observed at station OHI3 in Antarctica. The abovementioned station STHL shows an improvement of 0.15 ns (approximately 13%). We also observe the stations with stability deterioration, mainly distributed in North America. Comparing the GRW and GRN solutions, the differences in the GPS receiver DCB stability are smaller than 0.04 ns, which means that no significant improvement is found with the GRW solution relative to the GRN solution.

Influence on the GLONASS satellite-station link SPRDCB

In the GRW solution, the GLONASS satellite-station link SPRDCB is directly estimated. In the GRN solution, the GLONASS satellite DCB and the GLONASS receiver DCB are estimated separately. The GLONASS receiver DCB is actually a mean value that ignores the satellite-dependent part of the receiver IFDCB. The GLONASS SPRDCB with the GRN solution can also be recovered by adding the

GLONASS satellite DCB and the GLONASS receiver DCB. The influence of the GLONASS receiver IFDCB consideration on the GLONASS satellite-station link SPRDCB can be obtained by subtracting the GRN recovered SPRDCB from the GRW estimated SPRDCB with the following equation:

$$dSPRDCB_i^l = SPRDCB_{GRW,i}^l - (DCB_{GRN}^l + DCB_{GRN,i}^l) \tag{10}$$

where $dSPRDCB_i^l$ is the GLONASS SPRDCB difference for each satellite-station link.

We selected six IGS stations to analyze the GRW estimated SPRDCB and the GRN recovered SPRDCB and their differences. These six stations are equipped with different receivers and antenna types most commonly used in the IGS network. These stations are ABMF with a TRIMBLE NETR9 receiver and TRM57971.00 antenna, ALIC with a LEICA GRX1200GGPRO receiver and LEIAR25.R3 antenna, BADG with a JAVAD TRE_G3TH DELTA receiver and JAVRINGANT_DM antenna, GODZ with a JPS EGGDT receiver and AOAD/M_T antenna, KIRU with a SEPT POLARX4 receiver and SEPCHOKE_MC antenna and URUM with a TPS NETG3 receiver and TPSCR3_GGD antenna.

Figure 9 shows the GLONASS satellite-station link SPRDCB for the six stations on DOY 75, 2014. The GRN recovered SPRDCB and GRW estimated SPRDCB are shown in the top and bottom plots, respectively. In the GRN solution, one GLONASS receiver DCB is estimated at one station, i.e., the receiver DCB differences between different

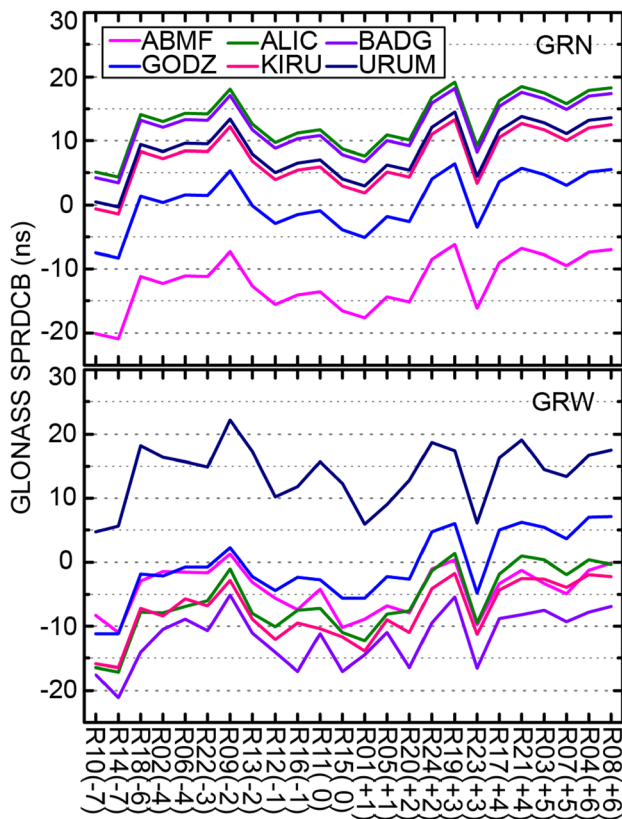


Fig. 9 GRN recovered SPRDCB (top) and the GRW estimated SPRDCB (bottom) for different GLONASS satellite-station links at six stations. The GLONASS satellites are listed in order of frequency channel

stations are the same for all satellites, so the GRN recovered SPRDCB for different stations show parallel lines. In the GRW solution, the common part and the satellite-dependent part of the GLONASS receiver IFDCB are considered. The GLONASS receiver IFDCB for different satellites at one station are different, so the parallel characteristics of the GLONASS SPRDCB for different stations disappear. In our experiment, the GLONASS SPRDCB at one station for different satellite-station links vary within 15 ns. The difference of GLONASS SPRDCB for the same satellite between two stations can reach up to 25 ns.

The GLONASS SPRDCB difference between the GRW solution and the GRN solution on DOY 75, 2014, is shown in Fig. 10. The SPRDCB difference represents the satellite-dependent part of the GLONASS receiver IFDCB. In our experiment, the SPRDCB difference for different stations has significantly different values. The minimum value of approximately -27 ns is observed for R16 at station BADG, and the maximum value is 12 ns for R10 at station ABMF. This indicates that the neglect of the satellite-dependent part of the GLONASS receiver IFDCB may introduce an error of 27 ns or 50 TECU in the STEC computation. At one station,

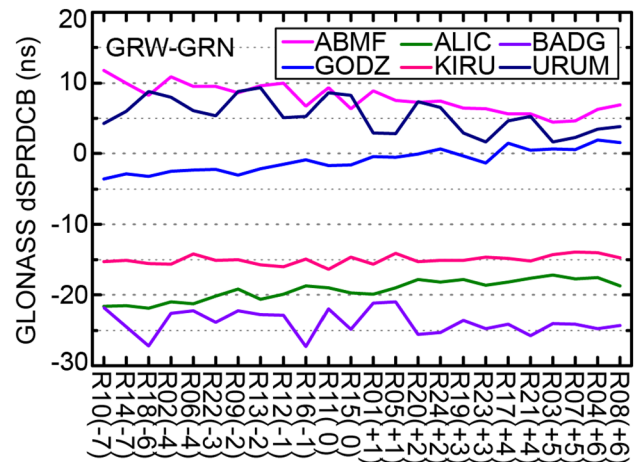
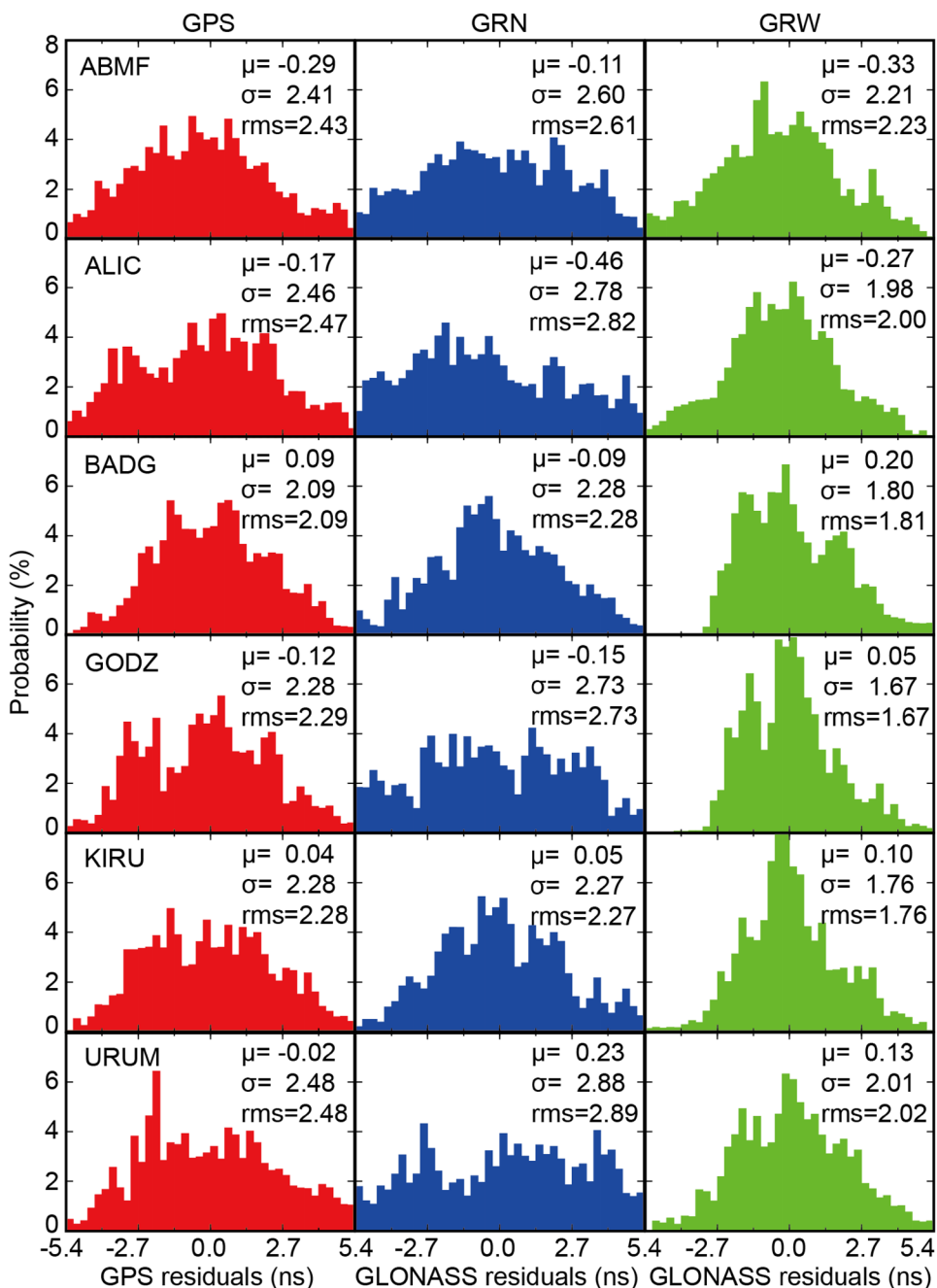


Fig. 10 GLONASS SPRDCB difference between the GRW solution and the GRN solution. The GLONASS satellites are listed in order of frequency channel

the difference of the GLONASS dSPRDCB between different satellites can be 7.7 ns, approximately 2.3 m. Therefore, it is necessary to consider the GLONASS receiver IFDCB in the positioning domain due to the very large inconsistency of the GLONASS receiver IFDCB corrections for all observed satellites. We also find that the GLONASS dSPRDCB at stations ABMF, ALIC and GODZ have correlations with the frequency channel, but no obvious correlations are found at the remaining three stations.

Furthermore, the parameters estimation residuals with the three solutions are presented in Fig. 11. The middle and right columns show the GLONASS residuals with the GRN and GRW solutions, respectively. In contrast, the GPS residuals with the GPS solution are shown in the left column. In the GPS solution, the GPS residuals are mainly normally distributed for the six stations. The biases range from -0.29 to 0.09 ns, and the STDs range from 2.09 to 2.48 ns. Compared with the GPS residuals, the GLONASS residuals with the GRN solution have larger STDs due to the inaccurate mean value estimation of the GLONASS receiver IFDCB. The STDs for stations ABMF, ALIC, BADG, GODZ, KIRU and URUM are 2.60, 2.78, 2.28, 2.73, 2.27 and 2.88 ns, respectively. In the GRW solution, the STDs of the GLONASS residuals decrease rapidly at all stations. The GRW solution shows 15.0%, 28.8%, 21.1%, 38.8%, 22.5% and 30.2% improvements in the STD at each station compared to the GRN solution. The STDs of the GLONASS residuals with the GRW solution are even smaller than those of the GPS residuals. It is confirmed that considering the GLONASS receiver IFDCB can help improve the precision of the estimated parameters.

Fig. 11 Parameters estimation residuals with the three solutions. The left, middle, and right columns represent the GPS residuals with the GPS solution, the GLONASS residuals with the GRN solution, and the GLONASS residuals with the GRW solution, respectively. The μ , σ and rms represent bias, STD and RMS, respectively



Influence on the global ionospheric VTEC map

The influence of the GLONASS data and the receiver IFDCB consideration on the global ionospheric VTEC map is analyzed in this section. Figure 12 shows the global VTEC map differences between the GPS, GRN and GRW solutions at 12:00 UTC on DOY 75, 2014. The VTEC differences between the GRN and GPS solutions range from -5 to 4 TECU. Most of the large differences are distributed over the regions where only a few stations are located. In

regions with many stations, such as the European continent, the VTEC differences are generally within 1 TECU. When we consider the GLONASS receiver IFDCB, the VTEC differences between the GRW and GPS solutions are smaller than those between the GRN and GPS solutions. Comparing the middle plot with the top plot, the apparently negative values at low latitudes are reduced. In the bottom plot, the VTEC differences between the GRW and GRN solutions are within 3 TECU and are mainly positive values at low and high latitudes. This indicates that the consideration of the

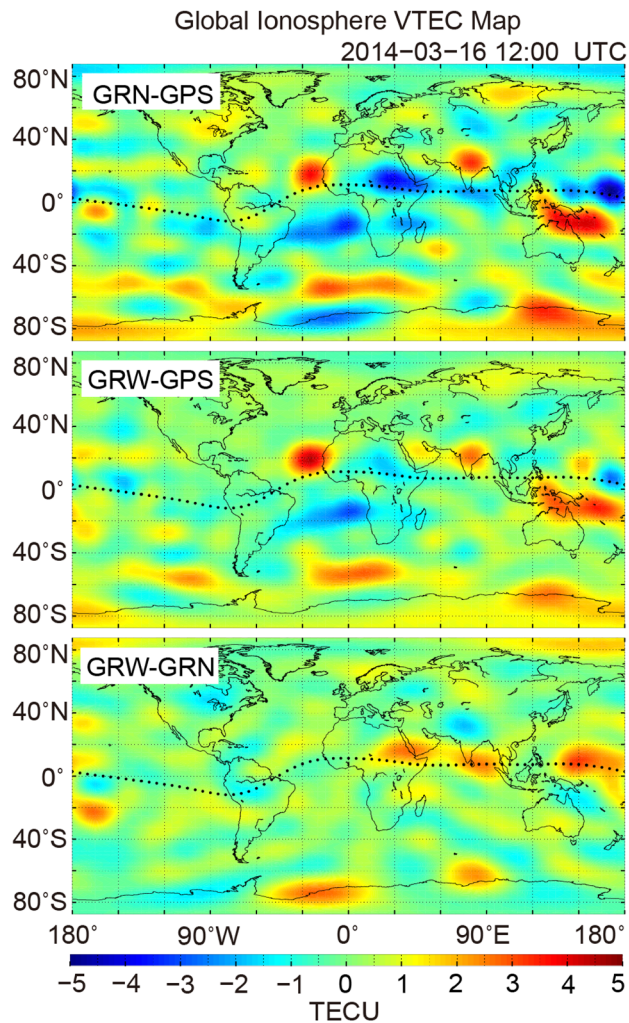


Fig. 12 Global ionospheric VTEC map differences between the GPS, GRN and GRW solutions at 12:00 UTC on DOY 75, 2014. The top, middle and bottom plots represent the differences between the GRN and GPS, between the GRW and GPS, and between the GRW and GRN, respectively

GLONASS receiver IFDCB has an influence on the magnitude but not the distribution of the VTEC differences.

The GIM product includes 13 global ionospheric VTEC maps for each day. We computed the biases and STDs of the VTEC differences between the three solutions. The VTEC biases and STDs from DOY 49 to 108 are shown in Fig. 13. The biases between GRN solution and GPS solution range from -0.2 to 0.2 TECU, while the biases between the GRW and GPS solutions range from 0.0 to 0.2 TECU. The apparent change is that the negative biases are generally eliminated. This result indicates that the introduction of GLONASS data with consideration of the receiver IFDCB can increase the VTEC values of the GIM by approximately 0.1 TECU. In the bottom plot, the STDs between the GRN and GPS solutions range from 1.1 to 1.6 TECU and those

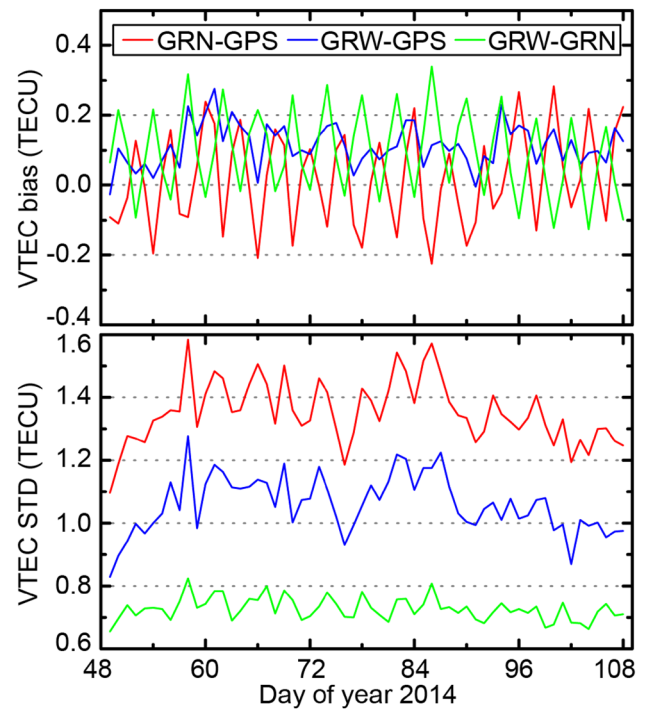


Fig. 13 VTEC biases (top) and STDs (bottom) between the GPS, GRN and GRW solutions from DOY 49 to 108. Red, blue and green represent the differences between the GRN and GPS solutions, between the GRW and GPS solutions, and between the GRW and GRN solutions, respectively

between the GRW and GPS solutions range from 0.8 to 1.3 TECU. Compared with the GRN solution, the STDs of the GRW solution are decreased by approximately 0.3 TECU. This means the GRW solution shows more consistency with the GPS solution than the GRN solution. Additionally, the average STD between the GRW and GRN solutions is 0.7 TECU, approximately 70% of the STD between GRW solution and GPS solution. This indicates that the consideration of the GLONASS receiver IFDCB also influences the VTEC map, but this influence is smaller than that induced by introducing the GLONASS data to global ionospheric modeling.

To validate the internal precision of the GIM, a self-consistency test was conducted in our experiment, i.e., comparing the GIM-derived VTEC with the GPS-based ionospheric VTEC (Li et al. 2015; Zhang and Zhao 2019). Specifically, the root mean square (RMS) at each station was calculated, and the daily RMS was a mean value over all stations. Then, the precision improvement IMP can be computed using $IMP = (RMS_{ref} - RMS_{eva}) / RMS_{ref} \cdot RMS_{eva}$ and RMS_{ref} and RMS_{eva} are the daily RMS of the evaluated solution and the reference solution, respectively. Figure 14 shows the internal precision of GPS, GRN and GRW solutions and the precision improvement from DOY 49 to 108. The RMSs of the three solutions range from 2.7 to 3.6 TECU. When the GLONASS data are introduced,

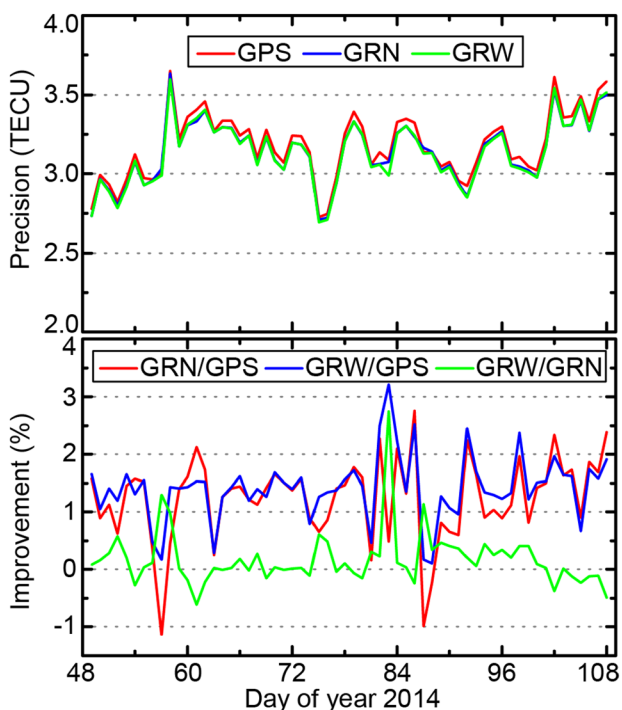


Fig. 14 Internal precision (top) of the GPS, GRN and GRW solutions and the precision improvement (bottom) of the GRN solution relative to GPS solution, the GRW solution relative to GPS solution and the GRW solution relative to GRN solution from DOY 49 to 108

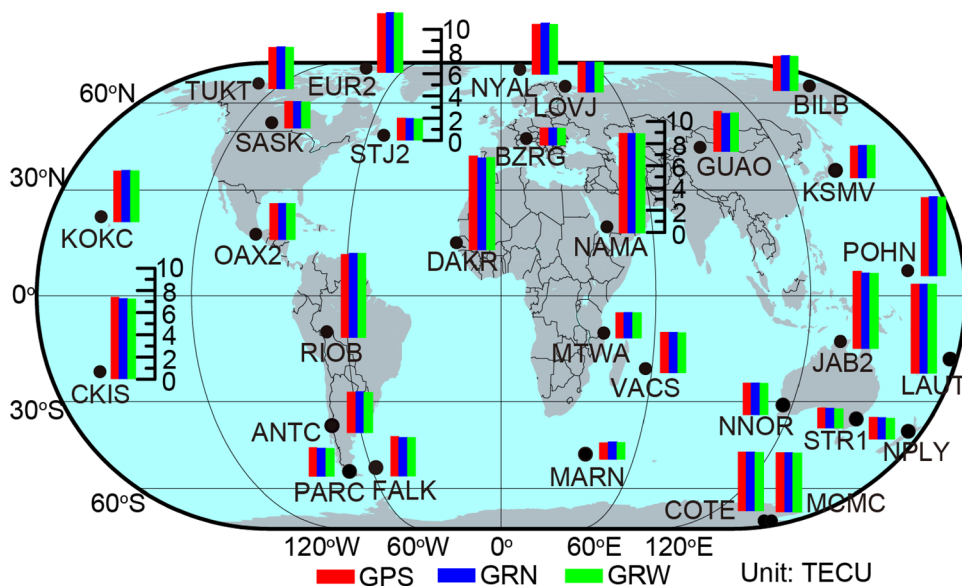
the internal precision of the GRN and GRW solutions is slightly better than that of the GPS solution. The average improvement of the GRN and GRW solutions relative to the GPS solution is approximately 1.3%. This indicates that the contribution of the GLONASS data to global ionospheric modeling on a global scale is small according to the internal precision test. Similarly, the contribution of the GLONASS receiver IFDCB consideration is also

very limited. However, it is also observed that the consideration of the GLONASS receiver IFDCB can revise the inaccurate estimation of the VTEC on some days, such as on DOY 57, 83 and 87. The results of our experiment show that the GRW solution is more reliable than the GRN solution.

Besides the internal precision test, an external accuracy test called dSTEC test (Hernández-Pajares et al. 2017) was conducted. We selected 30 IGS stations that were not used in our ionospheric modeling to assess the GPS-, GRN- and GRW-derived GIMs. The stations are globally distributed, as shown in Fig. 15. Similar to the internal precision test, we computed the RMS of the dSTEC test at each station for the GPS, GRN, and GRW solutions. The accuracy ranges from 1 to 9 TECU and is strongly correlated with the latitude. The accuracy at low latitudes is significantly larger than that at middle and high latitudes. The maximum RMS is approximately 9 TECU at station NAMA in Africa, and the minimum RMS is approximately 1.5 TECU at station BZRG in Europe.

The accuracy improvement at each station was also computed, as shown in Fig. 16. The stations are listed in order of latitude from the northern hemisphere to the southern hemisphere. It shows that when the GLONASS data is added, the GRN and GRW solutions show accuracy improvement relative to the GPS solution at 57% and 73% of the stations, respectively. The maximum improvement for the GRN and GRW solutions is approximately 5%. Comparing the GRW solution with the GRN solution, 90% of the stations show improvement, although the maximum improvement is only 3%. Notably, the accuracy at station MARN shows apparent degradation with the GRN solution. But this problem can be reduced significantly with the GRW solution. The results show that the introduction of GLONASS data can

Fig. 15 External accuracy of the dSTEC test at 30 IGS stations. The red, blue and green stand for the GPS solution, the GRN solution and the GRW solution, respectively



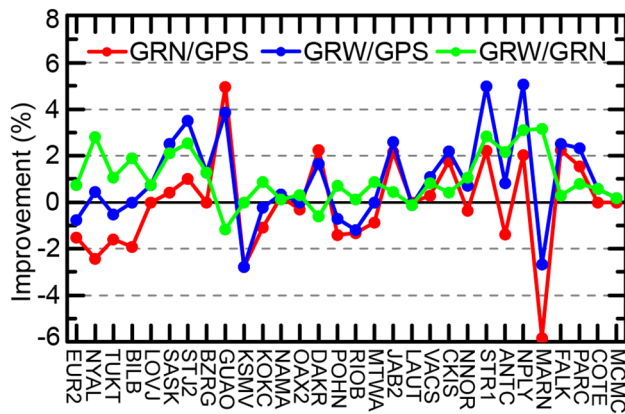


Fig. 16 Accuracy improvement at 30 IGS stations. The red, blue and green stand for the improvement of the GRN solution to the GPS solution, the GRW solution to the GPS solution, and the GRW solution to the GRN solution, respectively

improve the accuracy at most stations, and if we consider the GLONASS receiver IFDCB in further, more reliable global ionospheric models can be obtained.

Summary and conclusions

In this study, we specifically investigated the contribution of GLONASS data to global ionosphere mapping, especially considering the GLONASS receiver IFDCB. First, the characteristics of the GLONASS receiver IFDCB were analyzed based on a “co-located GNSS stations” experiment. The results show that the GLONASS receiver IFDCB is distinguishable from the leveling error induced by the CCL method and cannot be ignored in the data processing. Because the SD-DCB of two satellites on the same frequency channel show large differences, we suggest estimating the individual GLONASS receiver IFDCB for each satellite at one station. Second, we propose a modified model for combined GPS and GLONASS global ionosphere mapping. The GLONASS SPRDCB for each satellite-station link is directly estimated with the ionospheric model parameters in this modified model.

The influence of the GLONASS data and receiver IFDCB consideration on the DCB estimation and the global ionospheric VTEC map was comprehensively analyzed using data from the IGS network for DOY 49–108, 2014. The results show that the following (1) The inclusion of GLONASS data can improve the stability of the GPS satellite DCB by 3.8% and will increase the GPS receiver DCB at 77% of the stations compared to when only GPS data are used. (2) The GLONASS SPRDCB difference between the GRW estimated SPRDCB and the GRN recovered SPRDCB can be 27 ns, which means that the neglect of the

satellite-dependent part of the GLONASS receiver IFDCB may introduce an error of 50 TECU in the STEC computation. Considering GLONASS receiver IFDCB can reduce the GLONASS residual errors by approximately 26%. (3) The introduction of GLONASS data considering the receiver IFDCB will increase the VTEC map by approximately 0.1 TECU on a global scale. In the GIM internal precision test, the average improvement of the GRW solution relative to the GPS solution is approximately 1.3%. In the GIM external accuracy test, the GRW solution improves accuracy relative to the GPS solution at 73% of the stations.

It can be concluded that the introduction of GLONASS data, especially considering the GLONASS receiver IFDCB, will benefit global ionosphere modeling and DCB estimations for GPS and GLONASS. Although the contribution of the GLONASS data may not be significant on the global scale, the use of GLONASS data in regions with few IGS stations, such as in the southern hemisphere, still shows apparent improvement. When the GLONASS receiver IFDCB is considered in further, more reliable global ionospheric models can be obtained. This modified ionospheric model proposed in this study may be an alternative to the GNSS global ionosphere mapping.

Acknowledgements This research was partially supported by the National Natural Science Foundation of China (Grant No. 42030109), China Postdoctoral Science Foundation (Grant No. 2019M662715), the Fundamental Research Funds for the Central Universities (Grant No. 2042021kf0061), the Key Laboratory of Geospace Environment and Geodesy, Ministry of Education, Wuhan University (Grant No. 19-02-09), and LIEMARS Special Research Funding. The authors would like to acknowledge the IGS for providing the GPS and GLONASS data and IGS GIM products.

Author contributions Qiang Zhang and Jun Tao wrote the original manuscript and Xuanzuo Liu for validation, Zhigang Hu for methodology and editing, Qile Zhao for conceptualization and review. All authors reviewed the manuscript.

Data availability The GPS, GRN and GRW solution GIM products are available from the first author (zhangqiang@whu.edu.cn) or from the Wuhan University IGS Ionosphere Associate Analysis Center (<ftp://igs.gnsswhu.cn/pub/whu/MGEX/ionosphere>).

Declarations

Conflict of interest The authors declare no conflict of interest.

References

- Afraimovich EL, Yasukevich YV (2008) Using GPS–GLONASS–GALILEO data and IRI modeling for ionospheric calibration of radio telescopes and radio interferometers. *J Atmos Solar Terr Phys* 70(15):1949–1962
- Al-Shaery A, Zhang S, Rizos C (2013) An enhanced calibration method of GLONASS inter-channel bias for GNSS RTK. *GPS Solut* 17(2):165–173

- Brack A, Männel B, Wickert J, Schuh H (2021) Operational multi-GNSS global ionosphere maps at GFZ derived from uncombined code and phase observations. *Radio Sci* 56(10):e2021RS007337
- Chen Y, Yuan Y, Ding W, Zhang B, Liu T (2017) GLONASS pseudorange inter-channel biases considerations when jointly estimating GPS and GLONASS clock offset. *GPS Solutions* 21(4):1525–1533
- Ciraolo L, Azpilicueta F, Brunini C, Meza A, Radicella SM (2007) Calibration errors on experimental slant total electron content (TEC) determined with GPS. *J Geodesy* 81(2):111–120
- Coco DS, Coker C, Dahlke SR, Clynch JR (1991) Variability of GPS satellite differential group delay biases. *IEEE Trans Aerosp Electron Syst* 27(6):931–938
- Feltens J (2003) The activities of the ionosphere working group of the international GPS Service (IGS). *GPS Solut* 7(1):41–46
- Feltens J (2007) Development of a new three-dimensional mathematical ionosphere model at European space agency/European space operations centre. *Space Weather* 5(12):1–17
- Ghoddousi-Fard R (2014) GPS ionospheric mapping at natural resources Canada. In: IGS workshop 2014, 23–27 June, Pasadena, California
- Hernández-Pajares M, Juan JM, Sanz J (1999) New approaches in global ionospheric determination using ground GPS data. *J Atmos Solar Terr Phys* 61(16):1237–1247
- Hernández-Pajares M, Juan JM, Sanz J, Orus R, Garcia-Rigo A, Feltens J, Komjathy A, Schaer SC, Krankowski A (2009) The IGS VTEC maps: a reliable source of ionospheric information since 1998. *J Geodesy* 83(3–4):263–275
- Hernández-Pajares M, Roma-Dollase D, Krankowski A, García-Rigo A, Orús-Pérez R (2017) Methodology and consistency of slant and vertical assessments for ionospheric electron content models. *J Geodesy* 91(12):1405–1414
- Hernández-Pajares M, Lyu H, Garcia-Fernandez M, Orus-Perez R (2020) A new way of improving global ionospheric maps by ionospheric tomography: consistent combination of multi-GNSS and multi-space geodetic dual-frequency measurements gathered from vessel-, LEO- and ground-based receivers. *J Geodesy* 94(8):73
- Hernándezpajares M, Juan JM, Sanz J, Aragón-Angel A, García-Rigo A, Salazar D, Escudero M (2011) The ionosphere: effects, GPS modeling and the benefits for space geodetic techniques. *J Geodesy* 85(12):887–907
- IGSMail 4371 (2003) IGS GLONASS tracking data.
- Juan JM, Rius A, Hernández-Pajares M, Sanz J (1997) A two-layer model of the ionosphere using global positioning system data. *Geophys Res Lett* 24(4):393–396
- Li Z, Yuan Y, Li H, Ou J, Huo X (2012) Two-step method for the determination of the differential code biases of COMPASS satellites. *J Geodesy* 86(11):1059–1076
- Li Z, Yuan Y, Wang N, Hernandez-Pajares M, Huo X (2015) SHPTS: towards a new method for generating precise global ionospheric TEC map based on spherical harmonic and generalized trigonometric series functions. *J Geodesy* 89(4):331–345
- Liu T, Zhang B, Yuan Y, Li Z, Wang N (2019) Multi-GNSS triple-frequency differential code bias (DCB) determination with precise point positioning (PPP). *J Geodesy* 93(5):765–784
- Mannucci AJ, Wilson BD, Yuan DN, Ho CH, Lindqwister UJ, Runge TF (1998) A global mapping technique for GPS-derived ionospheric total electron content measurements. *Radio Sci* 33(3):565–582
- Montenbruck O, Hauschild A, Steigenberger P (2014) Differential code bias estimation using multi-gnss observations and global ionosphere maps. *Navigation* 61(3):191–201
- Nie W, Xu T, Rovira-Garcia A, Juan Zornoza JM, Sanz Subirana J, González-Casado G, Chen W, Xu G (2018) Revisit the calibration errors on experimental slant total electron content (TEC) determined with GPS. *GPS Solut* 22(3):85
- Ren X, Zhang X, Xie W, Zhang K, Yuan Y, Li X (2016) Global Ionospheric Modelling using Multi-GNSS: BeiDou, Galileo. *GLO-NASS and GPS Sci Rep* 6:33499
- Roma-Dollase D, Hernández-Pajares M, Krankowski A, Kotulak K, Ghoddousi-Fard R, Yuan Y, Li Z, Zhang H, Shi C, Wang C, Feltens J, Vergados P, Komjathy A, Schaer S, García-Rigo A, Gómez-Cama JM (2018) Consistency of seven different GNSS global ionospheric mapping techniques during one solar cycle. *J Geodesy* 92(6):691–706
- Schaer S (1999) Mapping and predicting the earth's ionosphere using the global positioning system. Ph.D. Dissertation, University of Berne
- Shi C, Yi W, Song W, Lou Y, Yao Y, Zhang R (2013) GLONASS pseudorange inter-channel biases and their effects on combined GPS/GLONASS precise point positioning. *GPS Solut* 17(4):439–451
- Vergados P, Komjathy A, Runge TF, Butala MD, Mannucci AJ (2016) Characterization of the impact of GLONASS observables on receiver bias estimation for ionospheric studies. *Radio Sci* 51(7):1010–1021
- Villiger A, Schaer S, Dach R, Prange L, Sušnik A, Jäggi A (2019) Determination of GNSS pseudo-absolute code biases and their long-term combination. *J Geodesy* 93:1487–1500
- Wang N, Yuan Y, Li Z, Montenbruck O, Tan B (2016) Determination of differential code biases with multi-GNSS observations. *J Geodesy* 90(3):209–228
- Wanninger L (2012) Carrier-phase inter-frequency biases of GLONASS receivers. *J Geodesy* 86(2):139–148
- Yao Y, Liu L, Kong J, Zhai C (2018) Global ionospheric modeling based on multi-GNSS, satellite altimetry, and Formosat-3/COSMIC data. *GPS Solut* 22(4):104
- Zhang Q, Zhao Q (2018) Global ionosphere mapping and differential code bias estimation during low and high solar activity periods with GIMAS software. *Remote Sens* 10(5):705
- Zhang Q, Zhao Q (2019) Analysis of the data processing strategies of spherical harmonic expansion model on global ionosphere mapping for moderate solar activity. *Adv Space Res* 63(3):1214–1226
- Zhang Q, Zhao Q (2023) Negative VTEC with spherical harmonic expansion model under different solar activity conditions. *Adv Space Res* 71(3):1806–1817
- Zhang R, Yao Y, Hu Y, Song W (2017a) A two-step ionospheric modeling algorithm considering the impact of GLONASS pseudo-range inter-channel biases. *J Geodesy* 91(12):1435–1446
- Zhang X, Xie W, Ren X, Li X, Zhang K, Jiang W (2017b) Influence of the GLONASS inter-frequency bias on differential code bias estimation and ionospheric modeling. *GPS Solut* 21(3):1355–1367
- Zhang B, Teunissen PJG, Yuan Y, Zhang X, Li M (2018) A modified carrier-to-code leveling method for retrieving ionospheric observables and detecting short-term temporal variability of receiver differential code biases. *J Geodesy* 93(1):19–28
- Zhang Z, Lou Y, Zheng F, Gu S (2021) On GLONASS pseudo-range inter-frequency bias solution with ionospheric delay modeling and the undifferenced uncombined PPP. *J Geodesy* 95(3):32

Publisher's Note Springer Nature remains neutral with regard to jurisdictional claims in published maps and institutional affiliations.

Springer Nature or its licensor (e.g. a society or other partner) holds exclusive rights to this article under a publishing agreement with the author(s) or other rightsholder(s); author self-archiving of the accepted manuscript version of this article is solely governed by the terms of such publishing agreement and applicable law.



Qiang Zhang is a postdoctoral researcher at the GNSS Research Center of Wuhan University. He received his Ph.D. degree from Wuhan University in 2019. His current research mainly focuses on GNSS ionosphere monitoring and analysis.



Jun Tao received his master's degree from Wuhan University, Wuhan, China, in 2019, where he is currently a Ph.D. candidate at the School of Geodesy and Geomatics. His main research interest is real-time GNSS positioning and its application.



Xuanzuo Liu is a master's candidate at the GNSS Research Center of Wuhan University. He received a bachelor's degree from the China University of Geosciences (Wuhan) in 2021. His current research focuses mainly on BDS performance evaluation and integrity monitoring.



Zhigang Hu is a professor at the GNSS Research Center, Wuhan University. He received his Ph.D. degree from Wuhan University in 2013. The focus of his current research lies in GNSS antenna phase center field calibration and BDS performance evaluation.



Qile Zhao is a professor at the GNSS Research Center of Wuhan University. He received his Ph.D. degree from Wuhan University in 2004. From 2006–2007, as a postdoctoral fellow, he did his postdoctoral program in DEOS, Delft University of Technology, the Netherlands. His current research interests are the precise orbit determination of GNSS and LEO satellites and high-precision positioning using GPS, Galileo and BDS.